



# A frequency Control Strategy for microgrid based on Fuzzy Logic

*Strategia kontroli częstotliwości zasilania mikro sieci w oparciu o koncepcję logiki rozmytej*

**Abstract.** A microgrid (MG) can classically operate with two modes, namely on-grid and off-grid modes. When a MG is connected to the main power, the stability of the voltage and the frequency is maintained by the main grid in term of letting all the inverters within the MG operate in PQ mode. However, once a disconnection occurs, the MG will run out of control. Therefore, it is necessary to keep the frequency and the voltage within the limit values by introducing a generator (such as a diesel) to play the role of the main grid. Additionally, this approach helps ensure the balance between energy production and consumption. In this paper, an intelligent control strategy has been proposed to control the frequency that guarantees the consumption to be in equilibrium with the generation, through adjusting active power by employing a fuzzy logic concept. The performance of the proposed strategy is evaluated by the simulation with various scenarios.

**Streszczenie.** Mikrosieć (MG) może klasycznie działać w dwóch trybach, mianowicie w trybie sieciowym i poza siecią. Gdy MG jest podłączony do głównego zasilania, stabilność napięcia i częstotliwości jest utrzymywana przez główną sieć, umożliwiając wszystkim falownikom w mikro sieci działanie w trybie PQ. Jednak po odłączeniu MG straci kontrolę. Dlatego konieczne jest utrzymanie częstotliwości i napięcia w granicach wartości granicznych poprzez wprowadzenie generatora (takiego jak diesel), który będzie pełnił rolę głównej sieci. Ponadto takie podejście pomaga zapewnić równowagę między produkcją energii a jej zużyciem. W tym artykule zaproponowano inteligentną strategię sterowania w celu kontrolowania częstotliwości, która gwarantuje równowagę między zużyciem a generacją, poprzez dostosowanie mocy czynnej przy użyciu koncepcji logiki rozmytej. Wydajność proponowanej strategii jest oceniana poprzez symulację z różnymi scenariuszami.

**Keywords:** Microgrid; Fuzzy logic; Storages; Photovoltaic.

**Słowa kluczowe:** Mikrosieć; Logika rozmyta; Magazyny; Fotowoltaika.

## Introduction

In the recent years, microgrids have emerged as a critical element in the evolution of modern electrical grids. A modern Microgrid (MG) is an integration of distributed energy resources (DER) (including PV, fuel cells, microturbines, etc.) with energy storage (such as energy capacitors, flywheels and batteries) and multiple electrical loads, are attracting a vast number of researchers. It can be operated in either stand-alone mode or grid-connected mode. The control of microgrid can be classified by coordinated and local control [1], [2], [3]. At the first glance, coordinated control aims to pick up the cost of energy production, the optimal power output among DER as well as the emission. Then, by making use of the forecast values of load demands, the electricity generation accompanied by the electricity price of the market in each hour of the next day, the optimal output power of DER, the cost, the consumption level of the utility grid, and the emission are estimated. On the other hand, intelligent local controllers can improve the efficiency of microgrid operations. Briefly speaking, both types of controllers are embedded in controlling the frequency and the voltage in both islanded mode and grid-connected mode. Moreover, in the transition state from the interconnected to islanded operations, the frequency and the voltage are also regulated efficiently [4].

In the literature, local control architecture is classified by centralized and decentralized schemes. In the centralized architecture, concentrated control is presented in [5]. In [6–7], a centralized control method shares power among DGs proportionally. Moreover, the precise power-sharing is obtained between microgrid s proportional to their ratings, too. There are several well-known methods applied to execute centralized control. In [8], An adaptive dynamic programming-based intelligent control strategy is developed for frequency stability in a microgrid utilizing renewable energy and energy storage.

In the decentralized control, the micro-source controllers (MCs) ' responsibility is to optimize the micro sources to achieve the demand, and to supply the maximum possible export power to the grid concerning the current prices of the market. In this control scheme, each micro-source controller is not able to gain the maximum revenue of the corresponding unit. However, the overall performance of the microgrid can be improved as presented in [4], [9]. In [10], the authors presented a decentralized control approach for frequency restoration and reactive power sharing in autonomous microgrids. The decentralized secondary control restores the microgrid frequency to its nominal value while ensuring accurate power sharing through droop control by employing the consensus protocol in [11]. In isolated AC microgrids, a decentralized secondary control method can allocate power and restore frequency without requiring communication in [12]. Beside that some energy storage-based controllers have been introduced in the literature. For instance, in [13-17], a BESS-based controller was presented to restore the voltage and frequency in a microgrid. On the other hand, model predictive control (MPC) is an effective method that predicts the future real power output of microgrid. In detail, the MPC method is applied to provide torque compensation for the reloaded wind turbine generators (WTGs) that participate in the frequency regulation in [18]. In [19], the MPC method is also adapted to adjust various parameters such as output voltage, frequency and power of the inverters in the multi-microgrid system. The  $H^\infty$  control method is employed as a secondary control strategy to maintain system frequency stability and to regulate both voltage and frequency, ensuring they remain close to their reference values [20]- [24].

In this paper, a new microgrid architecture including storage and PV energy is presented to maintain the frequency in the given limits according to the normal operating condi-

tions. Herein, the fuzzy logic is embedded in the proposed controller. In the proposed method, the frequency is not only a function of power but also of the state of charge and the initial operating conditions. To evaluate the performance of the proposed method, the simulation is executed in two scenarios, which are the islanded mode and the transition from the grid-connected to the islanded mode.

### System description and its control schemes

A modern microgrid, which is described in Figure 1 is composed of many components such as microturbine, PV, wind generator, fuel cell, and BESS. In which, each distributed energy resource relates to its corresponding bus (DC bus) via a power-electronic converter. The microgrid is connected to the main grid via the point of common coupling (PCC). Herein, by a substation transformer, the power is provided from a low-voltage (LV) transmission grid.

The operation of a microgrid can be classified in two modes, namely the grid-connected mode and the islanded mode. In the grid-connected mode, the PCC is closed, and the microgrid is connected to the upstream network. As a result, the microgrid can exchange energy with the main grid. In case that the disturbance occurs, or the microgrid gets the optimal operation state, the switch at PCC can be opened to disconnect the microgrid. Thus, the microgrid can continue to operate in the so-called islanded mode.

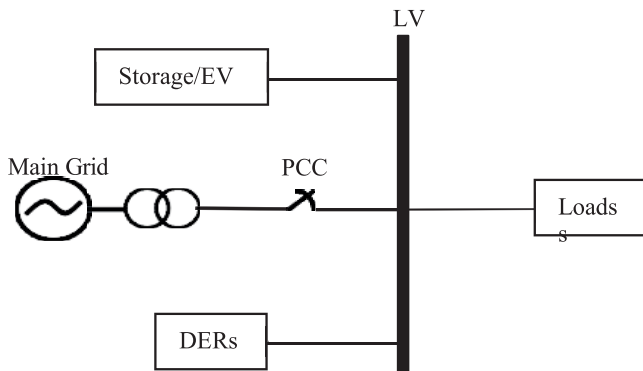


Fig. 1. A studied Microgrid structure

In this paper, the authors have studied a microgrid comprising PV system and Storage system that modelled as follows:

#### Photovoltaic system and its control scheme

A PV system is modelled by a current source in accompany with the power control. A simplified PV system model is determined as an injected current source with P/Q control to impose the active power and reactive power outputs following the values of  $P_{sp}$  (active power set-point) and  $Q_{sp}$  (reactive power set-point), respectively. The  $P_{sp}$  can be defined by the maximum power point tracker (MPPT) of the PV module and setting  $Q_{sp} = 0$ . More clearly, the operation diagram of an  $I_{abc}$  generation is illustrated in Figure 2, presented in [4].

In this Fig 2, from the measured voltage  $V_{mes}$  and measured current  $I_{mes}$ , the actual active power  $P_{act}$  and the actual reactive power  $Q_{act}$  can be deduced via P&Q calculation block as showed in following equations:

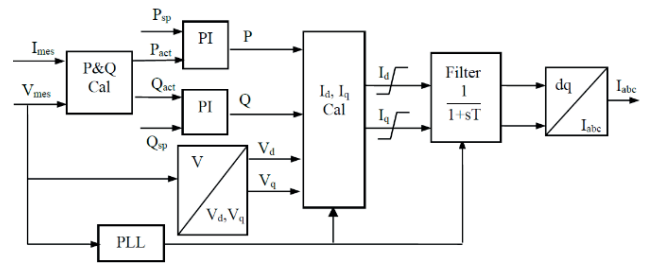


Fig. 2. PV system with power electronic interface P/Q control

$$(1) \quad P_{act} = V_{bc} \times i_c - V_{ab} \times i_a,$$

$$(2) \quad Q_{mes} = \frac{V_{bc} (2i_a + i_b) + V_{ca} (2i_b + i_a)}{\sqrt{3}}$$

Then, by making use of the PI controllers, the active power  $P$  and the reactive power  $Q$  can be estimated in term of tracking the corresponding reference values of  $P_{sp}$ ,  $Q_{sp}$ .

Simultaneously, direct voltage  $V_d$  and quadratic voltage  $V_q$  are calculated as showed in equations (3) and (4) from measure voltage  $V_{mes}$  through a converter, which transforms the voltage in polar to Cartesian

$$(3) \quad V_d = \frac{V_c - V_b}{\sqrt{3}}$$

$$(4) \quad V_q = \frac{2}{3} \cdot (V_a - \frac{1}{2} V_b - \frac{1}{2} V_c)$$

After that, the direct current  $I_d$  and quadratic current  $I_q$  are estimated from  $P$ ,  $Q$ ,  $V_d$ ,  $V_q$  via a calculation block as follows:

$$(5) \quad I_d = \frac{2}{3} \cdot \frac{(P \cdot V_d + Q \cdot V_q)}{(V_d^2 + V_q^2)}$$

$$(6) \quad I_q = \frac{2}{3} \cdot \frac{(P \cdot V_q - Q \cdot V_d)}{(V_d^2 + V_q^2)}$$

Finally, these estimated currents are filtered before getting into a dq-abc converter to infer the  $I_{abc}$ .

#### Storage system and its control scheme

A BESS is connected to the main grid through power electronics interface by which the power can be directly supplied to or taken out from the grid. In this paper, the battery's inverter can be controlled by a V/f controller. This controller includes the f/P and V/Q droop blocks which are determined by the droop coefficients ( $k$ ) and the P/Q controls. More clearly, the scheme of V/f controller is described in Figure 3

As can be seen in this Figure, the measured frequency  $f_{mes}$  and measured voltage  $V_{mes}$  are firstly compared with the corresponding reference values  $f_{ref}$ ,  $V_{ref}$ . Then, the estimated errors are employed to infer the relevant active power set-point  $P_{sp}$  and reactive power setpoint  $Q_{sp}$  via f/P droop block and V/Q droop block respectively. Herein, these estimated parameters become the inputs for P/Q control which are described in previous subsection.

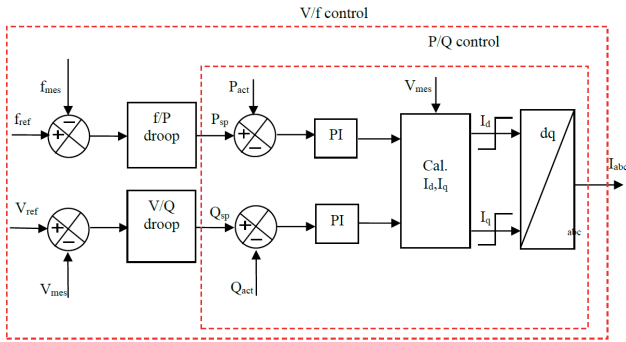


Fig. 3. Battery model with power electronic interface V/f control

In this study, the authors have focused on how to generate  $P_{sp}$  and  $Q_{sp}$  by proposing a method to determine the relevant droop coefficients  $k$ .

### Methodology

An electrical network architecture is composed of renewable energy and distributed energy storage. This storage can take the form of an electric vehicle (EV). In this case, sources and storages (such as the EVs) participate to regulate the voltage and the frequency in term of maintaining the stability of the network. The intelligent control of storage for frequency adjustment in the case of a normal operation (grid-connected mode) or islanded mode is proposed. The frequency regulation method focuses on the physical constraints of the storage such as the state of charge (SOC) of the batteries and the initial operating conditions. The principle of the control strategy is based on fuzzy logic with the local measurements without costly communication needs.

This work aims to regulate the system frequency where the control regime and the droop coefficient calculation presented as following:

### Design requirements

Figure 4 shows the frequency control characteristic for storage inverters.

There are two operating modes for storage system:

- Grid-connected mode
- Islanded mode.

In the grid-connected mode, frequency regulation characteristic is divided into 3 zones:

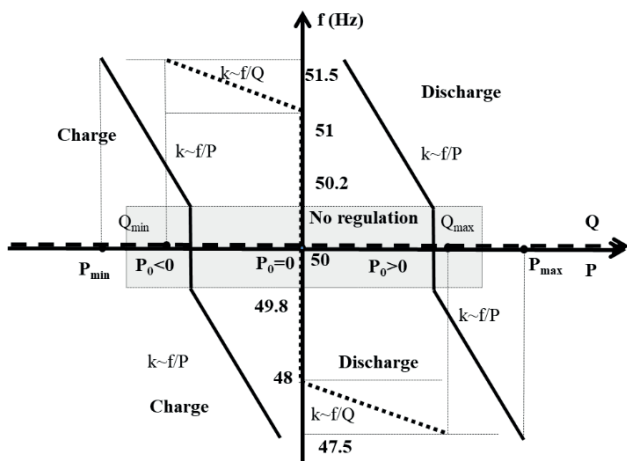


Fig. 4. PV system with power electronic interface P/Q control

- For  $49.8\text{Hz} \leq f \leq 50.2\text{Hz}$ , it is not able to regulate the system frequency, and the inverters (PV or storage) operate in the classical mode with  $Q = Q_0$  (or  $Q = 0$ ) and  $P = P_0$ .
- For  $47.5\text{Hz} \leq f \leq 49.8\text{Hz}$ , the storage inverters increase the active power discharge or reduce the active power load to raise the frequency.
- For  $50.2\text{Hz} \leq f \leq 51.5\text{Hz}$ , the storage inverters reduce the active power discharge or increase the active power load to lower the frequency.

In the islanded mode, all the storages participate in the frequency control by levelling the control scheme, via:

- level of primary frequency control, where the change of the frequency can be manage rapidly using droop control.
- level of secondary frequency control, where the storages and the PV sources join in to bring the frequency back to 50 Hz.

### Determination of the droop control coefficient k

The droop control coefficient  $k$  is determined by fuzzy logic as showed in Figure 5. In which, the value of  $k$  is adapted by the frequency state  $f_{mes}$ , the battery state of charge SOC<sub>mes</sub> and the active power  $P_{act}$ .

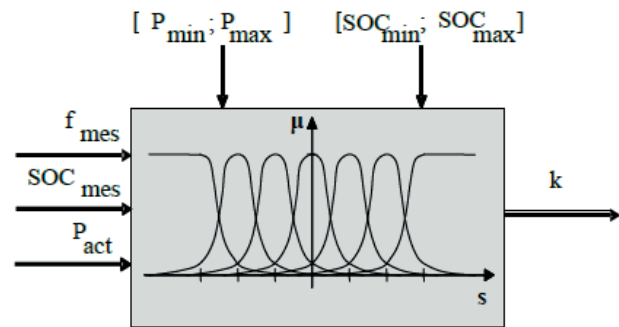


Fig. 5. Fuzzy Logic for the droop control frequency coefficient  $k$  determination

The  $k$  is obtained via the procedure including fuzzification stage and defuzzification stage:

### • Fuzzification

First and foremost, the initial conditions of the SOC are given by 2 modes of the battery (charge mode and discharge mode) as classified in Table 1.

Table 1. The initial operating conditions of BESS in 2 modes

| SOC        | 0–0.25 | 0–0.5 | 0.25–0.75 | 0.5–1 | 0.75–1 |
|------------|--------|-------|-----------|-------|--------|
| Definition | SOC-XS | SOC-S | SOC-M     | SOC-L | SOC-XL |

In which, the abbreviations are denoted as the level of capacity such as XS for X-small, S for small, M for medium, L for large and XL for X-large.

Then, the membership functions are defined as in Figure 6 based on the given information in Table 1

Next,  $P_0$  representing the initial power value of each storage in two modes are expressed in Tables 2, 3 and the membership functions are showed in Figure 7

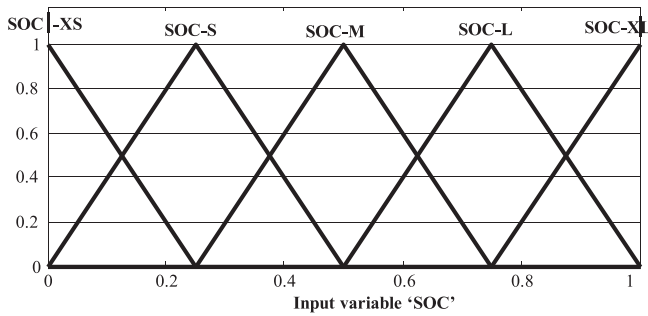


Fig. 6. Membership functions defined for fuzzy sets of input variable (SOC)

Table 2. The initial operating conditions of BESS in discharge mode

|            |        |       |           |       |        |
|------------|--------|-------|-----------|-------|--------|
| P0 (pu)    | 0–0.25 | 0–0.5 | 0.25–0.75 | 0.5–1 | 0.75–1 |
| Definition | P0-XS  | P0-S  | P0-M      | P0-L  | P0-XL  |

Table 3. The initial operating conditions of BESS in charge mode

|            |         |        |            |        |         |
|------------|---------|--------|------------|--------|---------|
| P0 (pu)    | -1–0.25 | -1–0.5 | -0.75–0.25 | -0.5–0 | -0.25–0 |
| Definition | P0-XS   | P0-S   | P0-M       | P0-L   | P0-XL   |

In Fig 7, the above sub-figure dedicates for the values of the initial power membership function in discharge mode, while the below sub-fig is noted for those in charge mode.

Then, via the fuzzy logic, the corresponding droop control coefficients to each level of SOC's capacity are estimated as illustrated in Figure 8.

### Defuzzification

In this stage, the fuzzy Inference table is inferred for two modes, which are discharge and charge as showed in Figure 9, where the above table is noted for discharge mode's fuzzy inference information each level of capacity of the SOC in consideration with the initial power value of each storage P0 while the below Table dedicates for the charge mode.

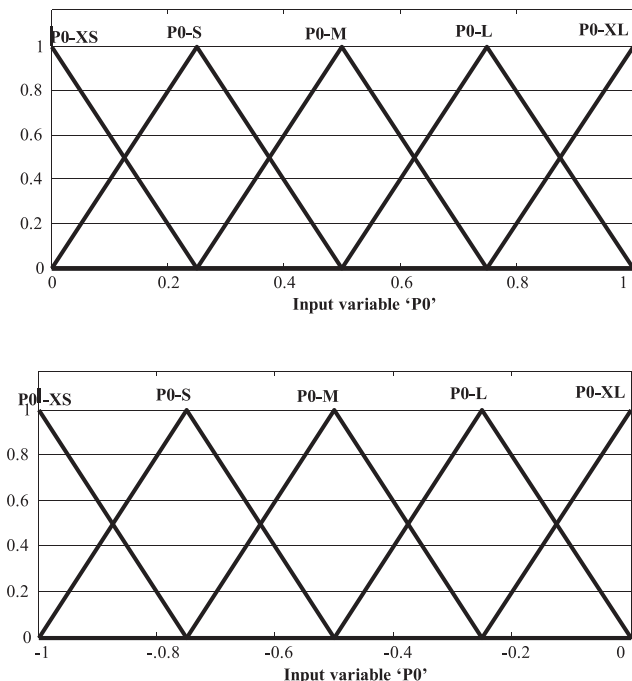


Fig. 7. Initial power membership functions of each storage in discharge and charge modes.

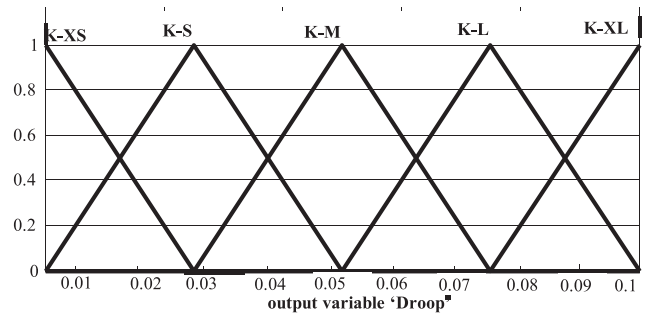


Fig 8. Membership functions defined for fuzzy sets of the 'droop' coefficient

| Fuzzy Inference table |       | SOC   |       |       |        |    |
|-----------------------|-------|-------|-------|-------|--------|----|
|                       |       | SOC-S | SOC-M | SOC-L | SOC-XL |    |
| P <sub>ini</sub>      | Po-XS | M     | M     | L     | XL     | XL |
|                       | Po-S  | S     | M     | L     | L      | XL |
|                       | Po-M  | S     | S     | M     | L      | L  |
|                       | Po-L  | XS    | S     | M     | M      | L  |
|                       | Po-XL | XS    | XS    | S     | M      | M  |

| Fuzzy Inference table |       | SOC   |       |       |        |    |
|-----------------------|-------|-------|-------|-------|--------|----|
|                       |       | SOC-S | SOC-M | SOC-L | SOC-XL |    |
| P <sub>ini</sub>      | Po-XS | M     | M     | S     | XS     | XS |
|                       | Po-S  | L     | M     | S     | S      | XS |
|                       | Po-M  | L     | L     | M     | S      | S  |
|                       | Po-L  | XL    | L     | M     | M      | S  |
|                       | Po-XL | XL    | XL    | L     | M      | M  |

Fig. 9. Fuzzy Inference Table for discharge mode and charge mode

### Simulation and results

The effectiveness of the suggested approach is assessed in this section through a case study of a rural network, as illustrated in Figure 10, where the whole network is supplied by a transformer of 250 kVA, 20/0.4 kV. By structure, it is composed of PV productions, single-phase and three-phase loads and BESS.

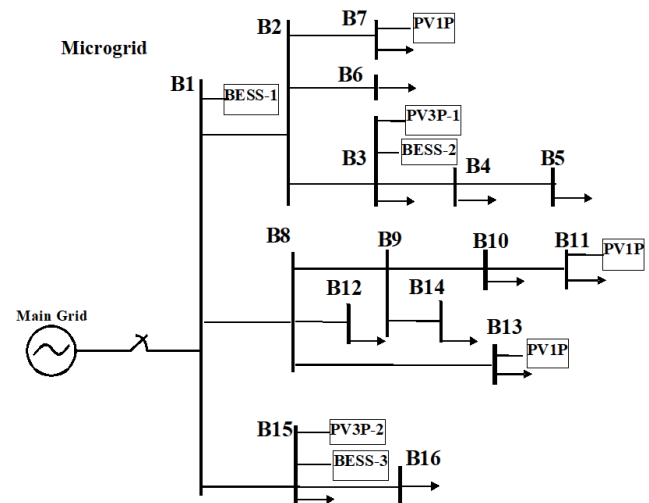


Fig. 10. The case-study's Microgrid architecture

### Scenario 1

At  $t = 2s$ , the MG is reversed to islanded mode. Before switching to islanded mode, the system comprises:

- + The total load is 75 kW
- + PV productions  $P_{PV3P-1} = 15 \text{ kW}$ ;  $P_{PV3P-2} = 20 \text{ kW}$ ;  $P_{PV1P} = 3 \times 5 \text{ kW}$
- + The power of the BESS: 0kW (in case of charge or discharge).
- + The main grid's power:  $P_{sys} = 25 \text{ kW}$

The MG starts to switch to the islanded mode at the moment of  $t = 2$  (seconds). In this stage, the frequency aims to be regulated at the nominal value. For instance, the PV pow-

Table 4. The four-case initial operating conditions of BESS

|          |            | BESS-1 | BESS-2 | BESS-3 |
|----------|------------|--------|--------|--------|
|          | $P_n$ (kW) | 30     | 30     | 30     |
| 1st Case | $P_{ini}$  | 0      | 0      | 0      |
|          | SOC        | 0.8    | 0.8    | 0.8    |
| 2nd Case | $P_{ini}$  | 0      | 0      | 0      |
|          | SOC        | 0.2    | 0.5    | 0.8    |
| 3rd Case | $P_{ini}$  | 0      | 5      | 10     |
|          | SOC        | 0.8    | 0.8    | 0.8    |
| 4th Case | $P_{ini}$  | 5      | 0      | -5     |
|          | SOC        | 0.2    | 0.5    | 0.8    |

er is kept to be a constant, while the power deficit is stood at (25kW) by the BESS to satisfy to load demand. Herein, the control strategy is to restore the varied frequency to the value of 50Hz by the BESS at the primary and the secondary level of the MG's hierarchical control structure. More clearly, the case study is carried out to evaluate the performance of the proposed method via three different BESS according to four cases suggested above. The initial conditions are showed in Table 4

- **1st Case:**
  - The BESS' initial power:  $P_{ini} = 0$ .
  - The SOC' initial values:  $SOC^1 = 0.8$ ,  $SOC^2 = 0.8$  and  $SOC^3 = 0.8$ .
- **2nd Case:**
  - The BESS' initial power:  $P_{ini} = 0$ .
  - The SOC' initial values:  $SOC^1 = 0.2$ ,  $SOC^2 = 0.5$  and  $SOC^3 = 0.8$ .
- **3rd Case:**
  - The BESS' initial powers:  $P_{ini1} = 0$ ,  $P_{ini2} = 5 \text{ kW}$  and  $P_{ini3} = 10 \text{ kW}$
  - The SOC' initial values:  $SOC^1 = 0.8$ ,  $SOC^2 = 0.8$  and  $SOC^3 = 0.8$ .
- **4th Case:**
  - The BESS' initial powers:  $P_{ini1} = 5$ ;  $P_{ini2} = 0 \text{ kW}$ ;  $P_{ini3} = -5 \text{ kW}$
  - The SOC' initial values:  $SOC^1 = 0.2$ ,  $SOC^2 = 0.5$  and  $SOC^3 = 0.8$ .

#### For the 1st case

In Figs 11 and 12, the variations of the active power, and the frequency of the given MG are described. In particular,

the MG and the main grid are discontinued from the moment of time  $t = 2s$ . From this moment, the frequency varies. Then, three BESS ( $Sto_1$ ,  $Sto_2$ ,  $Sto_3$ ) are discharged at the same value of power to obtain the load demand as presented in Figure 11. Since all BESS are given with the same initial conditions, the frequency is respected to be kept in the given permitted limit. As can be seen in the Figure 12, the frequency is rapidly brought back at 50Hz after the actions of the BESS' control strategy proposed.

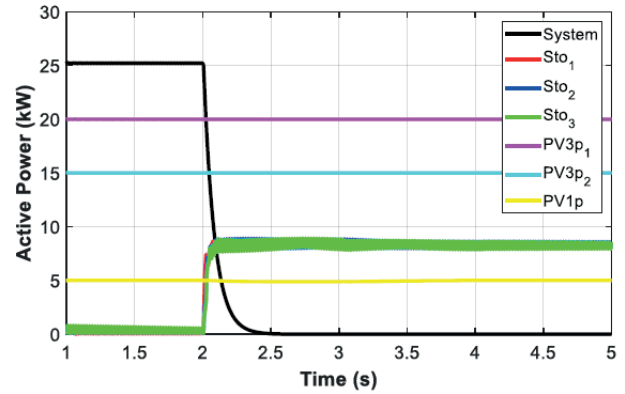


Fig. 11. The performance of the MG's active power in the 1st case

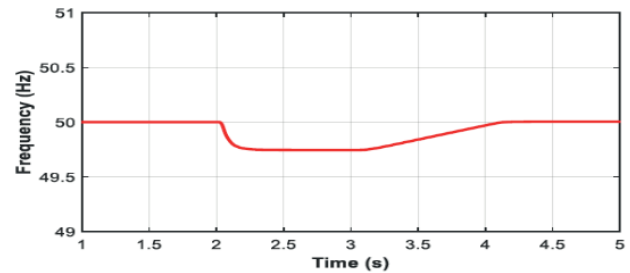


Fig. 12. The performance of the MG's frequency in the 1st case

#### For the 2nd case

Figs 13 and 14 show the variations of the active power and the frequency due to the disconnection between the MG and the main grid. Distinguishing from the 1st case, three BESS are adjusted with different values of power as presented in Figure 13. Since the  $Sto_3$  is defined by the largest initial capacitor ( $SOC^3 = 0.8$ ), thus the power deficit can be almost provided by this BESS. On the other hand, the  $Sto_1$  ( $SOC^1=0.2$ ) can provide the least power to the load demand

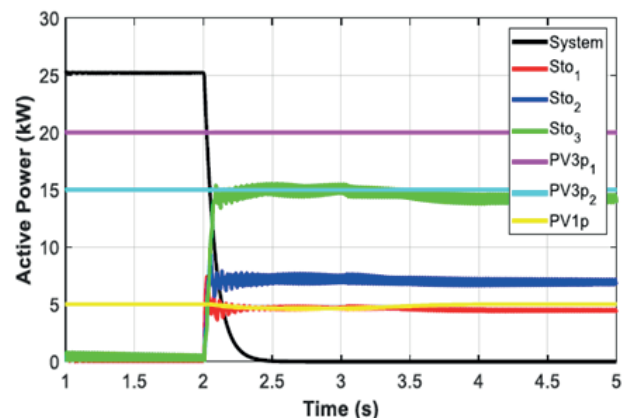


Fig. 13. The performance of the MG's active power in the 2nd case

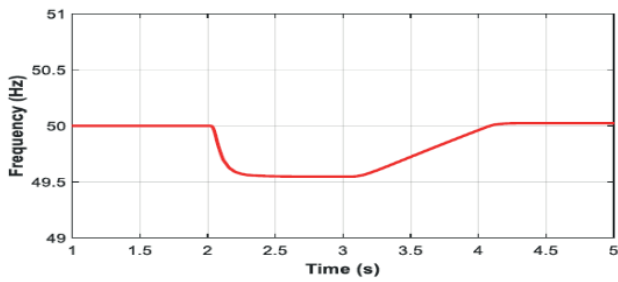


Fig. 14. The performance of the MG's frequency in the 2nd case

#### For the 3rd case

The performance of the active power and the frequency are presented in Figure 15 and Figure 16, respectively. Figure 15 describes that three BESS are given with the same value of the state of charge  $SOC^1 = SOC^2 = SOC^3$ , these discharge powers remain different due to their reliance on the original starting power of each BESS (that is, the power at  $t = 2s$ ). In Figure 7, the BESS-3's initial power ( $Sto_3$ ) is determined as the largest value ( $P_0=10kW$ ). However, the discharge power is calculated at the least value of 2.7kW. Conversely, the BESS-1 ( $Sto_1$ ) gains the largest power of 4.5kW. While Figure 16 illustrates that the frequency reaches the nominal value of 50Hz in comparison of the value of 50.02Hz in the 2nd case when the secondary control is considered.

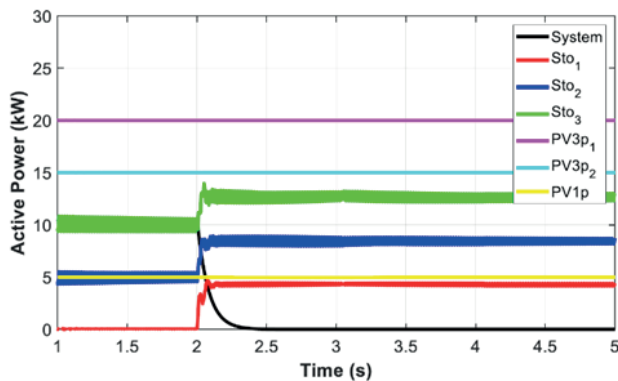


Fig. 15. The performance of the MG's active power in the 3rd case

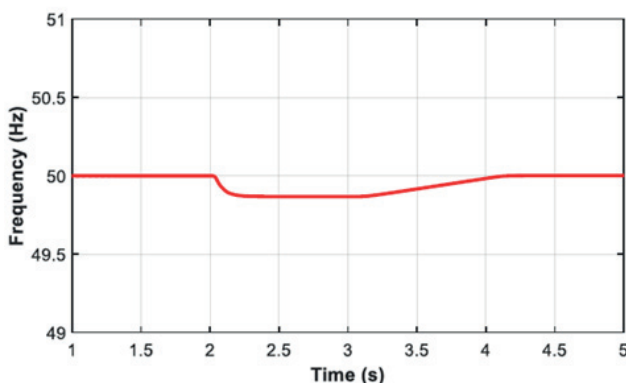


Fig. 16. The performance of the MG's frequency in the 3rd case

#### For the 4th case

The performance of the proposed method in the 4th case is illustrated in Figure 17 and Figure 18. In this case, the initial

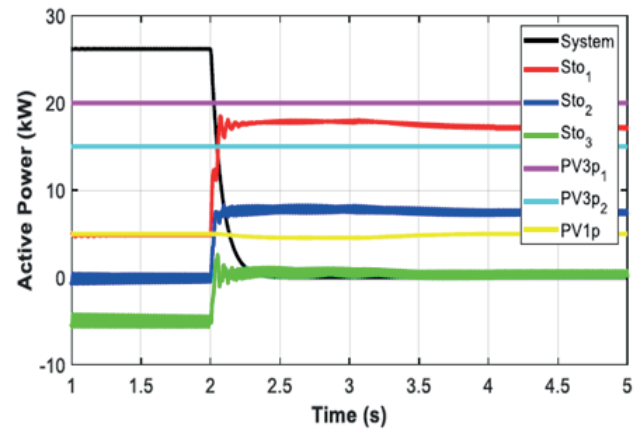


Fig. 17. The performance of the MG's active power in the 4th case

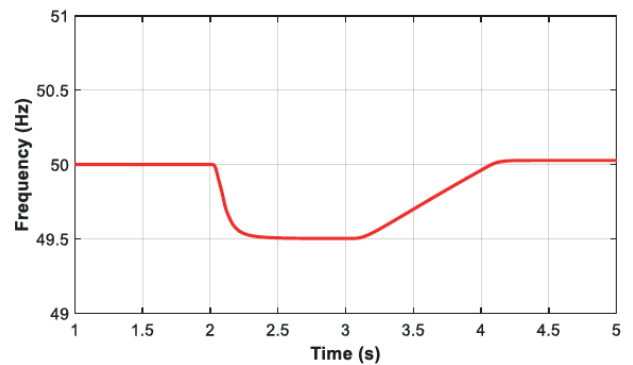


Fig. 18. The performance of the MG's frequency in the 4th case

states of three BESSs are defined as follows:

- + BESS-1 ( $Sto_1$ ) is discharged at  $P_{ini1} = 5kW$ ,
- + BESS-2 ( $Sto_2$ ) is in rest state with  $P_{ini2} = 0$ ,
- + BESS-3 ( $Sto_3$ ) is charged at  $P_{ini3} = -5kW$ .

In which, the discharge powers of these BESS are different as showed in Figure 17. After the modification, the BESS-3 quits charging. Then, it switches to the rest state. Otherwise, the BESS-1 and BESS-2 are discharged to meet for the demand loads. In this stage, BESS-1 supplies the most power. Figure 18 shows that the frequency is stabilized at the value of 50, 02Hz after the actions of primary and secondary control. As can be seen that the achievements of the 4th case seem to be the combination of the results of the 2nd case and the 3rd case.

#### Scenario 2

In this scenario, the variation of the PV productions is studied. For instance, it is reduced from 100% to 40% in the interval of time (3, 7), then increased from 40% to 90% from the moment of time  $t = 7s$ .

At first glance, the information is given as follows:

- + The total load is 75 kW
- + PV productions:
- $P_{PV3P_1} = 35 kW$ ;  $P_{PV3P_2} = 25 kW$ ;  $P_{PV1P} = 3 \times 5 kW$
- + 3 BESS (1<sup>st</sup>, 3<sup>rd</sup> and 15<sup>th</sup> nodes):
  - $Sto_1$ :  $P_{max} = 30kW$ ;  $Sto_2$ :  $P_{max} = 30kW$ ;  $Sto_3$ :  $P_{max} = 30kW$
- + The initial power values of the BESS are equal to zero in the case of charge or discharge.
- + The initial values of the SOC:  $SOC^1 = 0.8$ ,  $SOC^3 = 0.8$  and  $SOC^3 = 0.8$

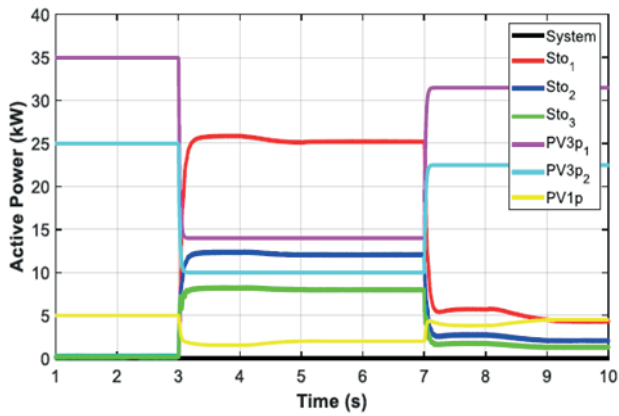


Fig. 19. The performance of MG's active power in the 2nd scenario

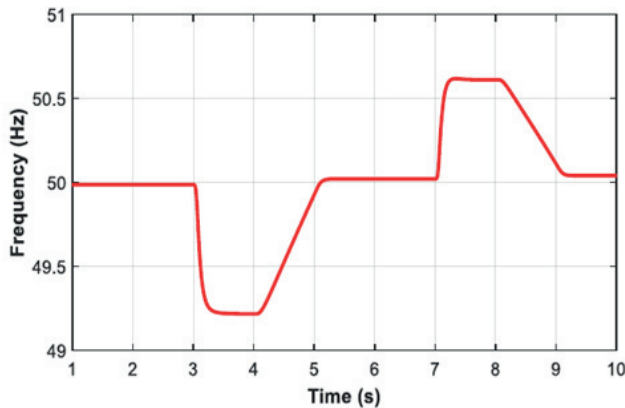


Fig. 20. The performance of MG's frequency in the 2nd scenario

Figure 19 and Figure 20 describe the performance of the proposed method in the 2nd scenario. In Figure 19, after

the reduction of the PV production from 100% to 40%, three BESS are discharged to maintain the balance between production and consumption. In which, the most power is supplied by the BESS-1 (Sto1) since this BESS has the largest initial capacitor ( $SOC^1 = 0.8$ ). Conversely, the BESS-3 (Sto3) is discharged with the least power since  $SOC^3 = 0.2$ . Figure 20 shows that the frequency is kept at 49.3Hz during the reaction of the primary control, then restored to 50 Hz after the action's secondary frequency control. Then, from the moment  $t = 7s$ , the PV production increases to 90% from 40%. As a result, the frequency is also increased to 50.55Hz. To overcome this issue, it is necessarily to reduce the discharge power. Finally, the frequency is maintained at the nominal value of 50 Hz after the performance of the primary and secondary control.

To summarize, we can see that the frequency of the system is always kept within the limits in both connected-grid mode and islanded mode. Furthermore, the microgrid is performed with maximize efficiency of the batteries. Thus, it increases the battery aging

## Conclusions

In this paper, an intelligent control method is proposed. The method makes it possible to maintain the frequency within the allowable limits in the normal operating conditions (connected to the network) or in the event of islanding with different operating modes. The main contribution of the proposed method is the employment of the fuzzy logic to adapt the control coefficient by considering the state of charge and the initial conditions of the BESS. This makes it possible to maximize the performance of the batteries and to minimize the constraints of battery aging. Moreover, this is a local method, with local information without the need for communications

**Authors:** Ngoc An LUU. University of Da Nang – University of Science and Technology

## REFERENCES

- [1] Lakshmi Satya Nagasri D. and Marimuthu R., Review on advanced control techniques for microgrids, *Energy Reports*, (2023), vol 10, pp.3054–3072.
- [2] An, L.N. and Tuan, T.Q., Dynamic Programming for Optimal Energy Management of Hybrid Wind–PV–Diesel–Battery, *Energies*, (2018), vol 11, pp.30–39.
- [3] Shahgholian G., A brief review on microgrids: Operation, applications, modeling, and control, *International Transactions on Electrical Energy Systems*, (2021), vol 31, pp. e12885.
- [4] Luu Ngoc An., Control and management strategies for a Microgrid, PhD dissertation, Grenoble University, France, 2014.
- [5] Jiefeng HU., Advanced Control in Smart Microgrids, PhD dissertation, University of Technology, Sydney, Australia, 2013.
- [6] S. Habibnia, M. Saeed Mahdavi, G. B. Gharehpetian, R. Ahmadihangar, A. Rosin and D. Vinnikov., A New Master-Slave based Centralized Control Method for an AC Microgrid with Multiple Distributed Energy Resources, *Proc. IEEE 13th International Symposium on Power Electronics for Distributed Generation Systems (PEDG)*, (2022), pp. 1–6.
- [7] R. Babazadeh-Dizaji, M. Hamzeh and A. Hekmati., Power Sharing in Multiple DC Microgrids Based on Concentrated Control, *Electrical Engineering (ICEE)*, (2018), 1304–1309.
- [8] C. Mu, Y. Zhang, H. Jia and H. He., Energy Storage Based Intelligent Frequency Control of Microgrid With Stochastic Model Uncertainties, *IEEE Transactions on Smart Grid*, (2020), vol. 11, no. 2, pp. 1748- 1758.
- [9] Kaczorowska, Dominika., Power flow control algorithm in a microgrid with energy storage. *PRZEGLĄD ELEKTROTECHNICZNY*, (2021). 7. 118–121
- [10] Zhang, Z.; Dou, C.; Yue, D.; Zhang, B.; Luo, W., A decentralized control method for frequency restoration and accurate reactive power sharing in islanded microgrids, *J. Frankl. Inst.*, (2018), 355, pp.8874- 8890.
- [11] Y. Khayat et al., Decentralized Frequency Control of AC Microgrids: An Estimation-Based Consensus Approach, *IEEE Journal of Emerging and Selected Topics in Power Electronics*, (2021), vol.9, no. 5, pp. 5183–5191.
- [12] Yang, P.; Xia, Y.; Yu, M.; Wei, W.; Peng, Y., A decentralized coordination control method for parallel bidirectional power converters in a hybrid ac-dc microgrid, *IEEE Trans. Ind. Electron*, (2018), 65, pp.6217–6228.
- [13] Faisal, M.; Hannan, M.; Ker, P.J.; Hussain, A.; Mansur, M.; Blaabjerg, F., Review of energy storage system technologies in microgrid applications: Issues and challenges, *IEEE Access*, (2018), vol 6, pp. 35143–35164.
- [14] Parise, G.; Martirano, L.; Kermani, M.; Kermani, M., Designing a power control strategy in a microgrid using pid/fuzzy controller based on battery energy storage, *Proc. IEEE IC&CPS Europe*, (2017), pp.1- 5.

- [15] Kermani, M., Transient voltage and frequency stability of an isolated microgrid based on energy storage systems, *Proc. IEEEIC*, (2016), pp.1–5.
- [16] Alshehri, Jaber and Khalid, Muhammad and Alzahrani, Ahmed., An Intelligent Battery Energy Storage-Based Controller for Power Quality Improvement in Microgrids, *Energies*, (2019), vol 12, pp.1–21.
- [17] Nirdesh Singh, Dinesh Kumar Jain, Energy storage participation for frequency regulation of microgrid in PV-dominated power system, *International Journal of Applied Power Engineering*, (2025), vol 14, No 1, pp.109–117
- [18] Wang H, Yang J, Ma Y, et al., Model predictive control of PMSG- based wind turbines for frequency regulation in an isolated grid, *IEEE 3rd international future energy electronics conference and ECCE Asia*, (2017), pp.1536–1541.
- [19] John T and Ping Lam S., Voltage and frequency control during microgrid islanding in a multi-area multi-microgrid system", *IET Generation, Transmission & Distribution*, 2017, vol 11, pp. 1502–1512.
- [20] Zhang, Y., Peng, C. Adaptive  $H_\infty$  event-triggered load frequency control in islanded microgrids with limited spinning reserve constraints. *Prot Control Mod Power Syst*, (2023), vol 8, pp. 30–43.
- [21] Lakshmi Satya Nagasri D., Marimuthu R., Review on advanced control techniques for microgrids, *Energy Reports*, (2023), vol 10, pp. 3054–3072.
- [22] G. K. Suman, J. M. Guerrero and O. P. Roy, Robust Frequency Control in Interconnected Microgrids: An  $H_2/H_\infty$  Control Approach, *IEEE Systems Journal*, (2022), vol 16, pp. 2044–2055
- [23] Bevrani H, Feizi MR and Ataei S., Robust frequency control in an islanded microgrid:  $H_{inf}$  and  $\mu$ -synthesis approaches, *IEEE Transactions on Smart Grid*, (2016), vol 7, pp.706–717.
- [24] Rezaei M. and Soltani J., Robust control of an islanded multi-bus microgrid based on input-output feedback linearisation and sliding mode control, *IET Generation, Transmission & Distribution*, (2015), vol 9, pp.2447–2484.